GMR
The Original

ULTRASOUND-ASSISTED GREEN SYNTHESIS OF CuO NANOPARTICLES USING BROWN MARINE MACROALGAE (*Padina tetrastromatica*) LOADED INTO STARCH/PVA ELECTROSPUN NANOSCAFFOLDS FOR CYTOCOMPATIBILITY AND ANTIOXIDANT ACTIVITY

Saravana Ganesh N[1], Sangeetha Nellore[2], Alagendran Subbarayalu[3]*

[1]Saveetha Medical College & Hospital (SMCH), Saveetha Institute of Medical and Technical Sciences (SIMATS), Thandalam, Chennai, Tamil Nadu 602105, India. nsg2479@gmail.com
[2]Saveetha College of Nursing (SCON), Saveetha Institute of Medical and Technical Sciences (SIMATS), Chennai 602105, Tamil Nadu, India. Email: hpdgurusangeetha@gmail.com
[3]Clinical Neuroscience and Phytomedicine Laboratory, Department of Research, Saveetha College of Nursing (SCON), Saveetha Institute of Medical and Technical Sciences (SIMATS), Chennai 602105, Tamil Nadu, India. Email: proteinblg@gmail.com; alagendrans.scon@saveetha.com. ORCID: https://orcid.org/0009-0009-0749-7180.
*Corresponding Author: proteinblg@gmail.com; alagendrans.scon@saveetha.com (A.S.)

ABSTRACT

Padina tetrastromatica extract-mediated green-synthesized copper oxide (CuO) nanoparticles (NPs) were incorporated into starch/polyvinyl alcohol (PVA) electrospun nanofibrous mats to develop a carbohydrate-based bioactive composite scaffold. The biosynthesized nanoparticles exhibited a characteristic UV-Visible absorption maximum at λ_max 273 nm, consistent with CuO NPs formation, which was further validated by FTIR and XRD analyses. Electrospinning of the starch/PVA/CuO system produced uniform, bead-free nanofibers indicating stable fiber formation governed by the polymeric network. *In vitro* cytocompatibility evaluation using 3T3-L1 fibroblast cells demonstrated high cell viability at the highest tested concentration (111%), confirming favorable short-term cellular responses. Antioxidant assays revealed concentration-dependent radical scavenging activity, with IC_{50} values of 42.82 ± 2.14 µg/mL (DPPH), 52.78 ± 2.64 µg/mL (nitric oxide), and 61.27 ± 3.06 µg/mL (superoxide) for the starch/PVA/CuO nanoscaffolds. Overall, these findings demonstrate that integrating green-synthesized CuO NPs within a starch-PVA electrospun matrix yields a cytocompatible scaffold with enhanced antioxidant performance, supporting its potential as a bioactive antioxidant scaffold platform for further biomedical evaluation.

KEYWORDS: *Padina tetrastromatica*, Green synthesis, CuO NPs, Starch/PVA-nanoscaffolds, Cytocompatibility and Antioxidant activity.

1. INTRODUCTION

The rapid development of nanotechnology has led to significant breakthroughs across diverse scientific and industrial fields, particularly in materials science, medicine, and environmental sustainability [1]. Among various nanomaterials, metal oxide nanoparticles have attracted substantial attention due to their distinctive physicochemical and biological properties [2]. Among them, copper oxide nanoparticles (CuO NPs) are emerging as a promising class of nanostructures with notable applications in catalysis, antimicrobial treatments, biosensors, and biomedicine [3]. The growing interest in CuO NPs stems from their cost-effectiveness, excellent chemical stability, high surface-area-to-volume ratio, and intrinsic antimicrobial and antioxidant potential [4].

Conventional chemical and physical methods for nanoparticle synthesis, while effective, often involve hazardous reagents, high energy demands, and generate toxic byproducts, posing risks to both the environment and human health [4]. To mitigate these drawbacks, recent advances have focused on green synthesis approaches that utilize biological entities such as plant extracts, fungi, bacteria, and algae as natural reducing and stabilizing agents [5]. These eco-friendly strategies align with the principles of green chemistry, promoting sustainability, safety, and scalability in nanoparticle fabrication [6].

Among biological sources, marine macroalgae have garnered considerable attention for nanoparticle synthesis due to their rich repository of bioactive phytochemicals, including polysaccharides, polyphenols, flavonoids, alkaloids, terpenoids, and proteins [7]. These compounds not only serve as effective reducing agents but also stabilize the nanoparticles by capping their surfaces [8]. *Padina tetrastromatica*, a brown macroalga commonly found along the coastal regions of the Indian Ocean, is particularly rich in such biomolecules [9]. Previous studies have reported its potent antioxidant, antimicrobial, and cytoprotective properties, attributed to its high content of phenolic acids and sulfated polysaccharides [10]. These unique biochemical attributes make *P. tetrastromatica* an ideal candidate for the biosynthesis of functional nanomaterials [11].

Ultrasonic-assisted extraction (UAE) of bioactive constituents from macroalgae enhances the efficiency of phytochemical release by disrupting cell walls through acoustic cavitation [12]. This technique is gaining momentum as a green and effective method to maximize yield and maintain the structural integrity of thermolabile compounds [13]. In this context, UAE-facilitated aqueous extraction of *Padina tetrastromatica* provides a potent and sustainable route for synthesizing CuO NPs with high biocompatibility and functionality [14].

To extend the biomedical utility of CuO NPs, especially for therapeutic applications such as wound healing and tissue regeneration, nanofibrous scaffolds have emerged as a favorable delivery platform [15]. Nanofibers mimic the extracellular matrix (ECM) architecture, offering high porosity, large surface area, and interconnectivity that support cell adhesion, proliferation, and nutrient exchange [16]. The electrospinning technique, known for its versatility and scalability, enables the fabrication of ultrafine fibers from various polymeric blends, producing scaffolds suitable for diverse biomedical purposes [17].

In this study, polyvinyl alcohol (PVA) was chosen as the primary electrospinnable polymer owing to its excellent film-forming properties, hydrophilicity, and biocompatibility [18]. However, to further improve the scaffold's biological profile and enhance its structural and mechanical integrity, natural starch was incorporated as a copolymer [19]. Starch, an abundant, biodegradable, and nontoxic polysaccharide, offers additional hydrogen bonding and reinforces the polymer matrix [20]. The integration of CuO NPs into the PVA/starch nanofibrous scaffolds creates a multifunctional system capable of combining physical support with bioactive functions such as antioxidation and cytoprotection [21].

The design and development of such CuO NP-loaded biopolymeric nanoscaffolds aim to leverage the synergistic effects of structural mimicry and bioactivity, making them highly relevant in biomedical domains, particularly in wound management, tissue regeneration, and localized therapeutic delivery [22]. The successful fabrication of these composite materials, however, requires rigorous physicochemical characterization to ascertain their morphology, crystalline structure, surface charge, thermal stability, and chemical interactions [23, 24].

Furthermore, the biocompatibility and safety of these materials must be assessed through in vitro cytotoxicity assays, such as the MTT test, using relevant mammalian cell lines [25]. The incorporation of CuO into scaffolds not only aims to improve structural features but also to imbue the materials with antioxidant capabilities, which are essential for counteracting oxidative stress in wound sites and promoting tissue recovery [15]. Although electrospun carbohydrate-based scaffolds are often explored for wound dressing applications, the present study is intended as a materials-focused proof-of-concept, emphasizing green synthesis, scaffold fabrication, and initial biological screening rather than full application validation.

While CuO NPs have been extensively explored in biomedical and antioxidant applications, comparatively less attention has been paid to the role of carbohydrate-based polymer networks in regulating nanoparticle behavior within electrospun scaffolds. In particular, starch-PVA blends are frequently employed to improve processability and biocompatibility; however, their hydrogen-bonded interactions and their influence on CuO NPs dispersion, stabilization, and redox-driven antioxidant performance remain insufficiently understood. Most reported PVA-starch/CuO NPs electrospun systems primarily emphasize fabrication and end-use applications, with limited discussion of how the carbohydrate network itself modulates structure–function relationships.

Given the abundance of hydroxyl groups in both starch and PVA, their combination is expected to form a semi-interpenetrating, hydrogen-bonded network during electrospinning. Such a network can influence solution rheology, fiber formation, nanoparticle immobilization, and accessibility of redox-active CuO surfaces, thereby affecting antioxidant activity and cytocompatibility. Understanding this carbohydrate-mediated modulation is essential for rational scaffold design, particularly when green-synthesized metal oxide nanoparticles are incorporated for bioactive functions.

Based on these considerations, this study hypothesize that, the starch-PVA hydrogen-bond network plays an active role in governing CuO NPs dispersion and antioxidant performance within electrospun nanofibrous scaffolds. Accordingly, the objectives of this study were to synthesize CuO NPs via an ultrasonic-assisted green route using *Padina tetrastromatica* extract, to fabricate CuO NPs-loaded starch/PVA electrospun nanoscaffolds and evaluate their physicochemical characteristics, and to assess the *in vitro* cytocompatibility and antioxidant efficacy of the resulting composite scaffold as a proof-of-concept bioactive platform.

2. MATERIALS AND METHODS

2.1. Materials

The study utilized *Padina tetrastromatica* macroalgae collected from Rameswaram, Tamil Nadu, India, for the green synthesis of CuO NPs, with copper(II) sulfate pentahydrate ($CuSO_4 \cdot 5H_2O$, Sigma-Aldrich) as the metal precursor. PVA (MW ~115,000) served as the primary electrospinning polymer, while starch (local supplier) enhanced scaffold properties. Analytical-grade reagents, including ethanol and Milli-Q water (Merck, Sigma-Aldrich), were used throughout. The HOLMARC HO-NFES-040 electrospinning system and syringe pump facilitated nanofiber fabrication. Characterization techniques included UV-Vis spectroscopy (VIS SPEC V-730), FT-IR (PerkinElmer Spectrum Two), XRD (Bruker D8 Advance), SEM (JEOL JSM-IT800 NANO), zeta potential and DLS (Malvern Zetasizer Ultra), and TGA (PerkinElmer TGA 8000). Biological evaluations employed 3T3-L1 cells for cytotoxicity assays, while DPPH, nitric oxide, and superoxide radical scavenging assays assessed antioxidant activity.

2.2. Marine Macroalgae Collection

The marine macroalga *Padina tetrastromatica* was gathered from the intertidal zones near Rameswaram, where it was thoroughly cleansed first with running tap water to remove sand and epiphytes, followed by multiple rinses with distilled water to ensure the elimination of residual salts and contaminants. After cleaning, roughly 100 grams of the algal biomass were manually cut into smaller fragments to facilitate uniform drying. These pieces were then spread in a shaded, well-ventilated area at ambient temperature for approximately 14 days to allow complete dehydration while preserving bioactive constituents. Once fully dried, the brittle algal material was pulverized into a homogeneous fine powder using an electric grinder, ensuring optimal particle size for efficient extraction in subsequent experimental procedures. This standardized preparation method maintained the integrity of the algal compounds while removing unwanted moisture and impurities.

2.3. UAE of Bioactive Compounds

To efficiently isolate bioactive compounds from *Padina tetrastromatica*, a precisely weighed quantity of 2 grams of the shade-dried and finely powdered algal material was taken and dispersed in 50 mL of ultrapure Milli-Q water. This suspension was subjected to UAE using a LABQUEST ultrasonic cleaner (Borosil; Serial No. 941032329018) set at 60 °C for a duration of 45 minutes. The ultrasonic waves facilitated cavitation effects, which helped in disrupting the algal cell walls, thus enhancing the release and solubilization of intracellular phytochemicals into the aqueous medium. After completion of the sonication process, the mixture was allowed to cool and then filtered through sterile Whatman No. 1 filter paper to remove solid residues and obtain a particle-free extract. The clear filtrate was stored in sterile conditions at 10 °C for immediate use in downstream synthesis. For long-term preservation, the filtrate was subjected to lyophilization using a laboratory-scale freeze-dryer to yield a stable powdered extract, which was stored in airtight containers for further experimental applications [26, 27].

2.4. Green Synthesis of CuO NPs

The eco-friendly biosynthesis of CuO NPs was carried out by employing the previously extracted algal filtrate as a reducing and stabilizing agent. A reaction mixture was prepared by adding 10 mL of *Padina tetrastromatica* extract-obtained by dissolving 10 mg of freeze-dried powder in 10 mL of Milli-Q water into 50 mL of 0.1 M copper sulfate pentahydrate ($CuSO_4 \cdot 5H_2O$) aqueous solution, maintaining a 5:1 volume ratio. The combined solution was continuously stirred at 650 revolutions per min (rpm) on a magnetic stirrer while maintaining a constant temperature of 60 °C for 2 h. A progressive color change from blue to bluish-green was visually observed, signifying the reduction of Cu^{2+} ions and the subsequent formation of CuO NPs. Upon completion of the reaction, the colloidal mixture was centrifuged at high speed, and the precipitate was washed three times with double-distilled water to remove any unreacted metal ions or residual phytochemicals. The resultant purified nanoparticles were lyophilized for 48 h to obtain a fine, dry powder and stored in desiccated conditions for future characterization and incorporation into scaffold systems [28].

2.5. Electrospinning of CuO-Embedded Starch/PVA Nanofibrous Scaffolds

The preparation of nanofibrous composite scaffolds embedded with CuO NPs was performed using the electrospinning technique. Initially, a 15% (w/w) aqueous solution of PVA was prepared by dissolving the polymer in Milli-Q water under constant stirring until a homogeneous and clear solution was obtained. To this solution, 100 mg of starch powder and 100 mg of the previously synthesized CuO NPs were added. The mixture was subjected to vigorous stirring at 50 °C for 2.5 h to ensure thorough mixing and uniform dispersion of NPs within the polymer matrix. The resulting solution was loaded into a syringe fitted with a stainless-steel needle with an internal diameter of 0.84 mm and mounted onto a HOLMARC HO-NFES-040 electrospinning apparatus. Electrospinning was conducted at room temperature under optimized conditions, including an applied voltage of 11.5 kV, a needle-to-collector distance of 12.3 cm, and a controlled feed rate of 0.4 mL/h. The process was run continuously for 6 to 8 h, resulting in the formation of uniform nanofibrous mats. The fabricated scaffolds were carefully peeled from the aluminum foil collector and preserved in a desiccator for subsequent physicochemical and biological assessments [18, 29, 30].

2.6. Physicochemical Characterization of Nanoparticles and Scaffolds

2.6.1. UV-Visible Spectroscopy

The optical characteristics and nanoparticle formation were evaluated using UV-Vis spectroscopy. Both CuO NPs and *Padina tetrastromatica* extract were analyzed using a VIS SPEC V-730 spectrophotometer, scanning over the wavelength range of 200 to 800 nm. Deionized water was used as the blank. The presence of distinct absorbance peaks, particularly due to surface plasmon resonance (SPR), confirmed the successful synthesis of CuO NPs [31].

2.6.2. Fourier Transform Infrared Spectroscopy (FTIR)

The chemical characterization of CuO NPs and their composite nanoscaffolds was conducted through FTIR spectroscopy using an ATR-equipped PerkinElmer Spectrum Two system. Spectra were acquired across the 4000–400 cm^{-1} wavenumber range at 4 cm^{-1} resolution, with each sample undergoing 64 cumulative scans to enhance signal clarity. The resulting absorption bands revealed distinct vibrational modes associated with hydroxyl (-OH) and phenolic groups from algal biomolecules, alongside carboxylate (C=O) stretches and characteristic Cu-O

lattice vibrations. These spectral features collectively confirmed the successful incorporation of CuO NPs within the polymeric matrix while preserving the organic functional groups responsible for NPs stabilization and antioxidant activity. The overlapping signatures of organic-inorganic interactions demonstrated effective integration of metallic and biological components in the hybrid scaffold system [32].

2.6.3. X-ray Diffraction (XRD) Analysis

The crystalline structure and phase purity of the fabricated NPs and composite scaffolds were examined through XRD studies performed on a Bruker D8 Advance system utilizing CuKα radiation (wavelength = 1.5406 Å). The instrument was operated at 40 kV and 40 mA, with diffraction data acquired across a 2θ angular range from 5° to 90° using an incremental step size of 0.029649°. The resulting diffraction profiles were systematically compared with reference patterns from the Joint Committee on Powder Diffraction Standards (JCPDS) database to identify the distinctive Bragg reflections corresponding to CuO crystallites. This analysis verified the formation of phase-pure CuO NPs and their successful integration within the scaffold matrix, as evidenced by the presence of characteristic peaks matching standard CuO diffraction patterns [33].

2.6.4. Scanning Electron Microscopy (SEM)

The structural characteristics of the samples, including surface topography, fibrous network organization, and spatial arrangement of NPs, were investigated using a JEOL JSM-IT800 NANO scanning electron microscope. To ensure optimal imaging conditions, all specimens underwent gold sputter-coating to improve surface conductivity. The obtained high-resolution micrographs revealed critical morphological details, demonstrating the consistency of fiber formation, successful incorporation of NPs within the matrix, and the three-dimensional porous architecture of the scaffold material. This analysis provided essential visual evidence of the material's microstructure and NPs distribution patterns [34].

2.6.5. Thermogravimetric Analysis (TGA)

The thermal properties and structural integrity of the starch/PVA-based electrospun nanoscaffolds were assessed via thermogravimetric analysis (TGA) using a PerkinElmer TGA 8000 instrument. Samples weighing approximately 5 mg were subjected to controlled heating from room temperature up to 550 °C, with a constant temperature increase of 15 °C per minute in a nitrogen-rich environment. The obtained weight-loss profiles revealed distinct thermal decomposition phases, including initial moisture evaporation, polymer breakdown, and final carbonaceous residue formation. These thermograms provided critical data on the material's moisture retention, thermal degradation thresholds, and ash content, enabling evaluation of the scaffold's heat resistance and long-term stability under biologically relevant conditions [35].

2.6.6. Zeta Potential and Particle Size Distribution

The colloidal characteristics, including hydrodynamic diameter and surface charge, of the CuO NPs were determined using the Malvern Zetasizer Ultra system. Zeta potential values provided information on the electrostatic stability of the NPs suspension. Particles with high absolute zeta potential values indicated good dispersion and minimized aggregation tendencies in aqueous media [32].

All experimental data, raw spectra, and processed outputs from these characterizations are publicly available on the Mendeley Data repository under the DOI: 10.17632/ddbgcpm32x.2.

2.7. *In Vitro* Cytotoxicity Evaluation

To assess the biocompatibility and cytotoxic effects of the algal extract, CuONPs, and CuO-loaded nanofibrous scaffolds, an in vitro MTT assay was performed using 3T3-L1 mouse preadipocyte cell lines. Cells were seeded in sterile 96-well plates at a density of 1×10^4 cells per well and incubated under standard conditions (37 °C, 5% CO_2) for 24 h to ensure cell attachment. Subsequently, the cells were exposed to varying concentrations (6.25, 12.5, 25, 50, and 100 µg/mL) of each test formulation for 24 h. Post-treatment, 10 µL of MTT reagent (5 mg/mL) was added to each well, followed by 4 h of incubation. The metabolically active cells reduced the yellow tetrazolium dye into insoluble purple formazan crystals. These crystals were dissolved using dimethyl sulfoxide (DMSO), and the absorbance was measured at 570 nm using a microplate reader. Cell viability was calculated as a percentage relative to untreated control cells [36].

2.8. Antioxidant Activity Assessment

2.8.1. DPPH Radical Scavenging Activity

The antioxidant potential of algal extract, CuO NPs, and starch/PVA/CuO NPs nanoscaffolds was measured using the DPPH (2,2-diphenyl-1-picrylhydrazyl) assay. Different sample concentrations were mixed with a 0.1 mM methanolic DPPH solution in equal proportions. The mixtures were incubated in darkness at room temperature for 30 minutes to reach equilibrium. Absorbance at 517 nm indicated scavenging activity, where reduced absorbance signified stronger antioxidant effects. Vitamin C acted as the reference standard. The percentage inhibition was calculated by comparing sample absorbance with the DPPH control. Triplicate experiments ensured data reproducibility.

2.8.2. Nitric Oxide (NO) Scavenging Activity

The NO scavenging ability of algal extracts, CuO NPs, and composite nanofibers was analyzed via the Griess reaction. Sodium nitroprusside (10 mM in PBS, pH 7.4) generated NO, which decomposed under physiological conditions. Test samples (25–100 µg/mL) were reacted with the NO solution at 25 °C for 2.5 h. Griess reagent

(0.33% sulfanilic acid in 20% acetic acid with 0.1% NEDD) detected nitrite ions, forming a purple chromophore measured at 540 nm. Activity was expressed relative to the control, using vitamin C as the standard.

2.8.3. Superoxide Anion ($O_2^{\bullet-}$) Scavenging Activity

Superoxide scavenging was evaluated using an NBT reduction assay. The reaction contained 0.2 mL NBT (1 mg/mL in DMSO), 0.6 mL test samples (25–100 µg/mL), and 2 mL alkaline DMSO (0.1 mL 5 mM NaOH in DMSO), totaling 2.8 mL. Superoxide radicals reduced NBT to purple formazan under alkaline conditions, quantified at 560 nm. Background absorbance was corrected using non-alkalized DMSO. Ascorbic acid was the reference, with results expressed in ascorbic acid equivalents (AAE) [37].

2.9. Statistical Analysis

All quantitative data obtained from experimental procedures were analyzed using SPSS version 25.0 and GraphPad Prism version 9.0 software. Results were expressed as mean values ± standard deviation (SD) based on triplicate independent trials. One-way analysis of variance (ANOVA) was employed to determine the statistical significance of differences among experimental groups. When applicable, Tukey's and Dunnett's post hoc tests were performed for pairwise comparisons. Statistical significance was established at a threshold of $p < 0.05$. Prior to ANOVA, the normality of data distribution was verified using the Shapiro–Wilk test. Pearson's correlation coefficient was also calculated to assess the relationship between experimental variables. All statistical interpretations were conducted at a 95% confidence interval [37].

3. RESULTS

3.1. UV–Visible Spectroscopy

The UV-Visible spectroscopy analysis of *Padina tetrastromatica* extract and CuO NPs was conducted using a JASCO V-730 spectrophotometer with a wavelength range of 200–800 nm, a data interval of 1 nm, and a bandwidth of 1.0 nm. The measurements were performed in absorbance mode with deionized water as the blank. The CuO NPs exhibited a distinct absorbance peak at 273 nm with an absorbance value of 0.547 (Fig. 1), which is indicative of surface plasmon resonance (SPR), confirming their successful synthesis. In contrast, the algal extract did not show a prominent peak in the provided data, suggesting differences in optical properties between the two samples. The instrumental parameters, including a scan speed of 1000 nm/min and baseline correction, ensured accurate and reproducible results. The absorption band observed around 273 nm is consistent with the formation of CuO NPs, as reported in previous studies. However, UV-Vis spectroscopy alone is not sufficient for definitive phase identification and is therefore interpreted in conjunction with FTIR and XRD analyses. Definitive confirmation of CuO formation is derived from characteristic Cu-O vibrational modes in FTIR spectra and phase-specific diffraction peaks observed in XRD analysis.

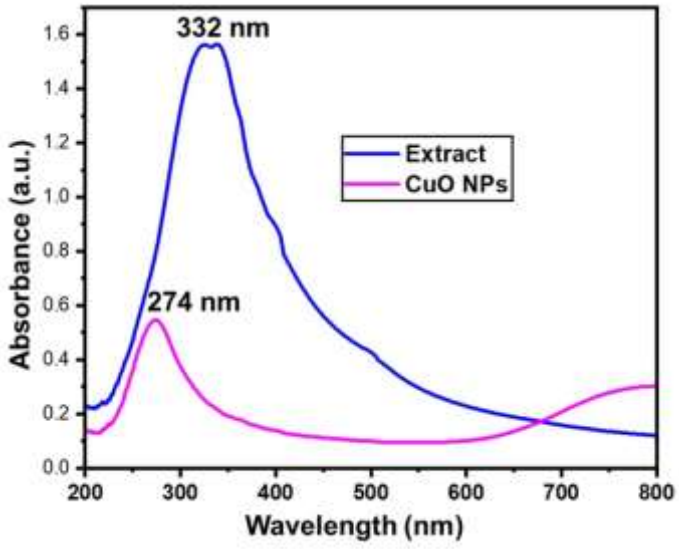

Fig. 1. UV-Vis absorption spectra of the *Padina tetrastromatica* extract and biosynthesized CuO NPs recorded in the range of 200–800 nm. The extract shows a characteristic absorption maximum at ~332 nm, while the CuO NPs exhibit a distinct peak at ~274 nm, confirming nanoparticle formation.

3.2. Fourier Transform Infrared spectroscopy

FTIR analysis of CuO NPs and starch/PVA electrospun nanoscaffolds was performed using a PerkinElmer Spectrum IR instrument in the range of 4000–400 cm^{-1}. The CuO NPs spectrum exhibited characteristic peaks (Fig. 2) at 602.84 cm^{-1} and 433.39 cm^{-1}, corresponding to Cu-O stretching vibrations, confirming the formation of metal-oxygen bonds. Additional peaks at 3136.73 cm^{-1} (O-H stretching) and 1654.94 cm^{-1} (C=O stretching) suggested the presence of hydroxyl and carbonyl groups, likely from residual organic compounds. The starch/PVA

nanoscaffolds displayed prominent peaks at 3297.44 cm^{-1} and 3258.67 cm^{-1} (O-H stretching), 1424.21 cm^{-1} (C-H bending), and 1108.87 cm^{-1} (C-O-C stretching), indicative of polysaccharide and PVA functional groups. Peaks below 1000 cm^{-1}, such as 940.79 cm^{-1} and 601.52 cm^{-1}, further confirmed polymer-metal interactions in the composite scaffolds. The spectral data collectively revealed the coexistence of organic functional groups (hydroxyl, carbonyl, and ether) from the biopolymers and inorganic Cu-O bonds, validating the successful integration of CuO NPs into the nanoscaffold matrix. The FTIR spectrum of the starch/PVA/CuO NPs nanoscaffold exhibits a broadened O-H stretching band and subtle shifts in C-O-C and C=O related vibrations compared to reported values for neat starch and PVA in the literature. Such band broadening and peak displacement are commonly associated with enhanced hydrogen bonding and polymer–polymer interactions in carbohydrate-based blends. The presence of CuO NPs may further influence these interactions by acting as coordination sites for hydroxyl groups, contributing to a stabilized hybrid network.

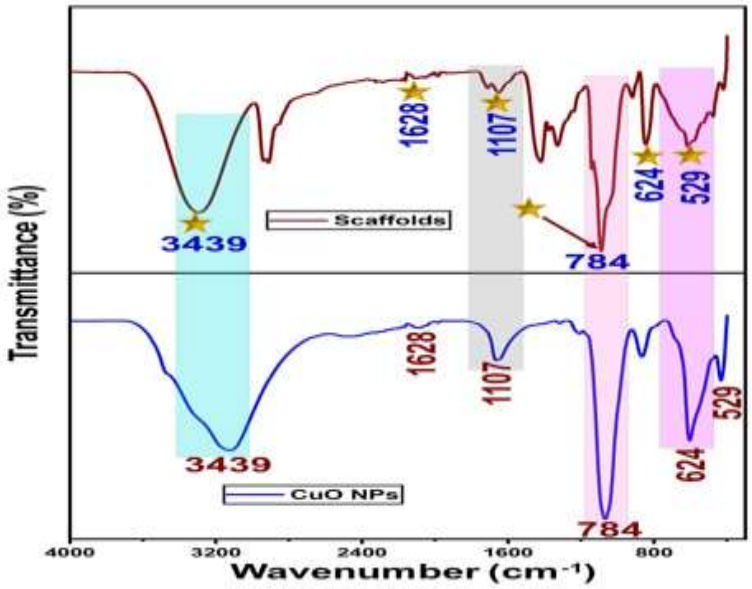

Fig. 2. FTIR spectra of CuO NPs and CuO NPs-loaded starch/PVA electrospun scaffolds (4000–400 cm^{-1}).

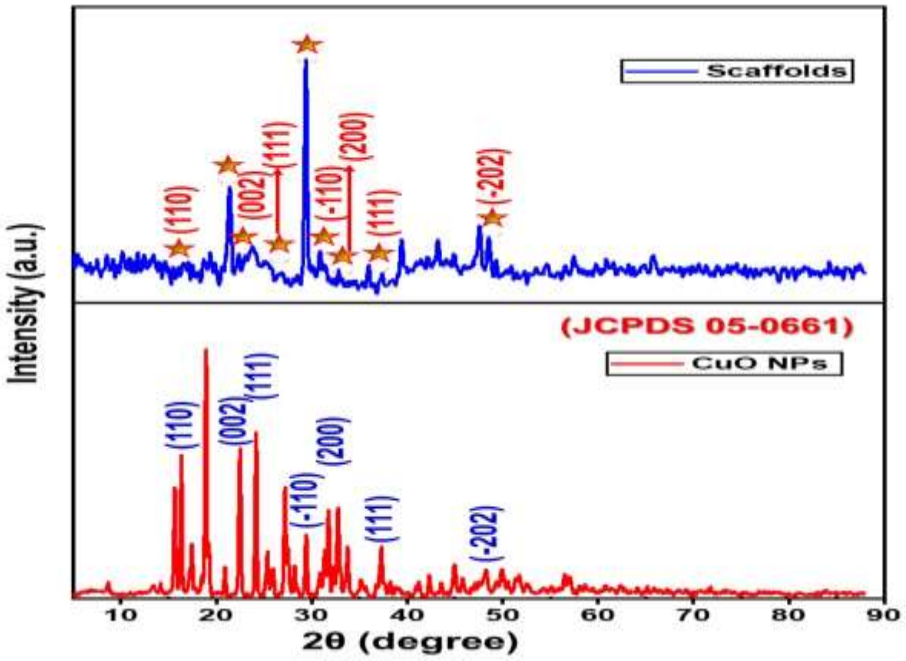

Fig. 3. XRD patterns of CuO NPs and CuO NPs-loaded starch/PVA electrospun scaffolds. The characteristic diffraction peaks indexed to the monoclinic CuO phase match the JCPDS card No. 05-0661, confirming phase-pure CuO and its successful incorporation within the polymer scaffold.

3.3. XRD analysis

XRD analysis of CuO NPs and starch/PVA electrospun nanoscaffolds was performed using a Bruker D8 Advance diffractometer with CuKα radiation (λ = 1.5406 Å). The CuO NPs exhibited prominent diffraction peaks at 2θ values (Fig. 3) of 13.310°, 15.601°, 16.321°, 17.433°, 18.938°, 20.836°, 22.537°, 24.173°, 25.351°, 25.874°,

27.118°, 28.165°, 29.408°, 31.894°, 32.745°, 33.661°, 35.101°, 37.260°, 38.242°, 41.121°, 42.233°, 43.477°, 44.916°, 45.898°, 48.188°, 49.955°, 51.656°, and 56.302°, corresponding to d-spacings ranging from 6.64656 Å to 1.63269 Å. The most intense peak at 18.938° (d = 4.68228 Å, relative intensity = 100%) confirmed the monoclinic tenorite phase of CuO (JCPDS 05-0661). The starch/PVA nanoscaffolds displayed a semi-crystalline structure with dominant peaks at 21.307° (d = 4.16681 Å, 39.0% relative intensity) and 29.349° (d = 3.04070 Å, 100% relative intensity), alongside minor peaks at 30.973°, 35.695°, and 39.384°, indicative of polymer crystallinity. The broader peaks and lower intensity in the nanoscaffolds suggested an amorphous matrix (82.9%) with embedded crystalline regions (17.1%), while the sharp, well-defined peaks of CuO NPs confirmed their high crystallinity. The absence of impurity peaks validated the phase purity of both materials, with the nanoscaffold's diffraction profile reflecting a composite structure integrating CuO NPs within the polymeric network.

3.4. SEM analysis

SEM analysis (Fig. 4) of CuO NPs and starch/PVA electrospun nanoscaffolds was conducted using a JEOL JSM-IT800 NANO instrument, with samples sputter-coated with gold to ensure optimal conductivity. The SEM micrographs revealed distinct morphological characteristics for both materials: the CuO NPs appeared as discrete, spherical to slightly irregular particles with a homogeneous size distribution, while the starch/PVA nanoscaffolds exhibited a highly porous, interconnected fibrous network with uniform fiber diameters, indicative of successful electrospinning. The nanofibers displayed smooth surfaces with occasional bead-free formations, and the embedded CuO NPs were uniformly dispersed within the polymeric matrix, confirming effective integration. The scaffold's architecture showed an open, three-dimensional structure with adequate porosity, which is favorable for cellular infiltration and nutrient diffusion in biomedical applications. High-resolution images further confirmed the absence of NPs aggregation, suggesting stable dispersion and compatibility between the CuO NPs and the polymer blend. These structural features collectively highlight the scaffold's potential for tissue engineering, where optimized morphology and NPs distribution are critical for functionality. The SEM results provide essential visual evidence of the successful fabrication of a nanocomposite system with desirable physical and topological properties.

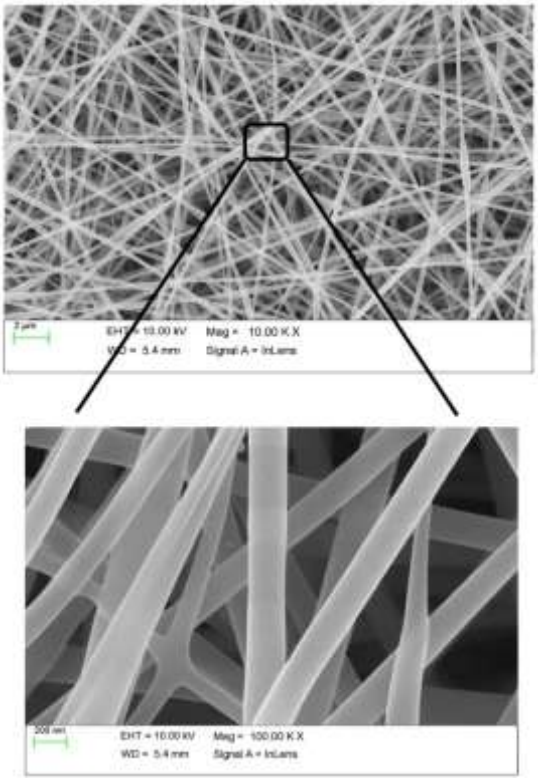

Fig. 4. SEM micrographs of CuO NPs-loaded starch/PVA electrospun nanofibrous scaffolds showing a randomly oriented, bead-free fibrous network. Low-magnification image (10.0 KX) highlights the interconnected porous architecture, while the high-magnification image (100.0 KX) reveals smooth fiber surfaces and uniform fiber morphology. Scale bars: 2 µm (top) and 200 nm (bottom); imaging conditions: EHT = 10 kV, WD = 5.4 mm.

3.5. TGA

The thermogravimetric profile of the starch/PVA/CuO electrospun nanoscaffolds is shown in Fig. 5. An initial minor mass loss below 150 °C corresponds to the removal of physically adsorbed moisture. The major degradation event occurs between ~250 °C and 420 °C, with an onset temperature of 298.21 °C and a peak degradation temperature of 356.55 °C, which is attributed to the thermal decomposition of starch and PVA polymer chains. The negative area (-41.912%) indicated significant weight loss during this phase, primarily attributed to the

decomposition of organic functional groups and polymer backbone scission. Within the investigated temperature range (up to 550 °C), the nanoscaffolds exhibit substantial mass loss associated with organic matrix degradation, confirming their biopolymeric nature. However, because the experiment was not extended beyond 550 °C, the residual mass at higher temperatures could not be determined, and therefore quantitative estimation of CuO content based on ash residue is not possible in the present study. Nevertheless, the observed degradation temperatures demonstrate that the incorporation of CuO NPs does not compromise the thermal stability of the starch/PVA matrix within the processing-relevant temperature window (<300 °C), which is suitable for biomedical scaffold fabrication and handling.

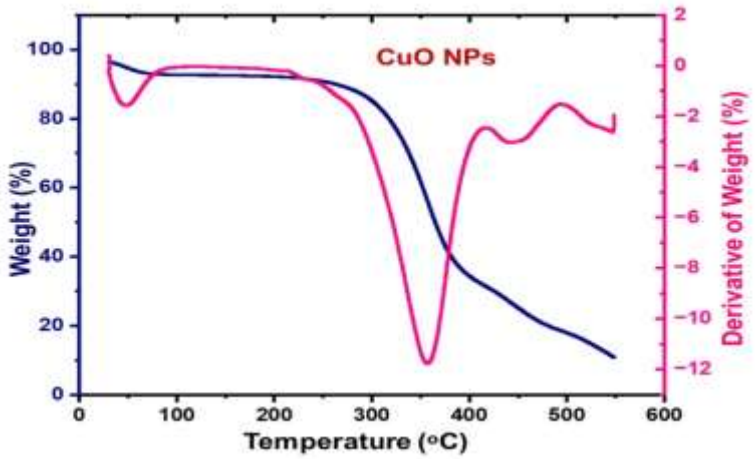

Fig. 5. TGA curve of starch/PVA/CuO NPs electrospun nanoscaffolds recorded from 30 °C to 550 °C at a heating rate of 15 °C min^{-1} under nitrogen atmosphere.

3.6. Zeta potential and particle size analysis

Dynamic light scattering analysis revealed a Z-average hydrodynamic diameter of 108 ± 1.4 nm, with a polydispersity index (PDI) of 0.312 ± 0.018, indicating a moderately polydisperse nanoparticle population (Fig. 6). The measured particle size reflects the hydrodynamic diameter of CuO NPs in aqueous dispersion, which includes contributions from solvation layers and surface-bound phytochemicals derived from the algal extract. Zeta potential measurements yielded an average surface charge of −22.13 ± 0.8 mV (Fig. 7). This negative surface charge suggests the presence of ionizable functional groups on the nanoparticle surface and provides moderate electrostatic stabilization against aggregation in aqueous media. However, as the absolute zeta potential value is below ±30 mV, the dispersion cannot be classified as highly stable and may exhibit limited aggregation over time. The apparent size differences observed between SEM, XRD, and DLS measurements arise from fundamental differences in measurement principles. SEM provides physical particle dimensions in the dry state, XRD estimates crystallite size, and DLS measures hydrodynamic diameter in suspension, which includes solvent and surface coatings. Therefore, the larger size observed in DLS measurements is expected and does not indicate inconsistency or aggregation artifacts. Based on these results, the CuO NPs dispersion is best described as moderately electrostatically stabilized under the measured conditions, rather than fully colloidally stable.

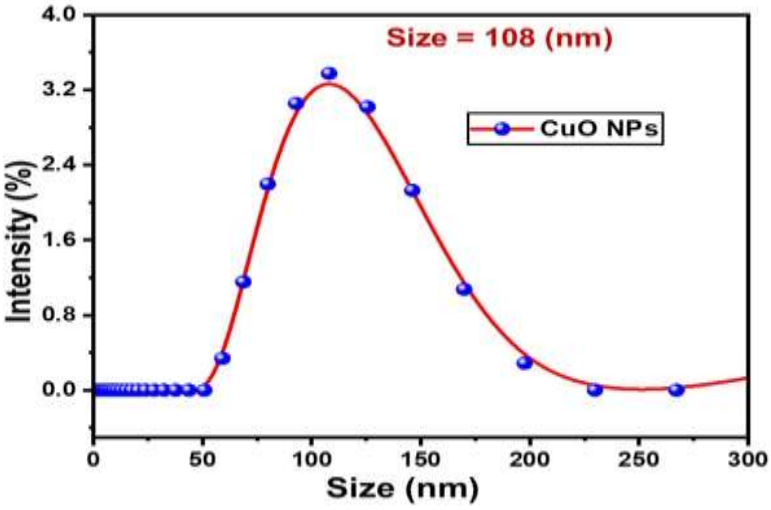

Fig.6. Intensity-weighted DLS size distribution of CuO NPs dispersed in Milli-Q water at 25 °C, showing Z-average hydrodynamic diameter and polydispersity.

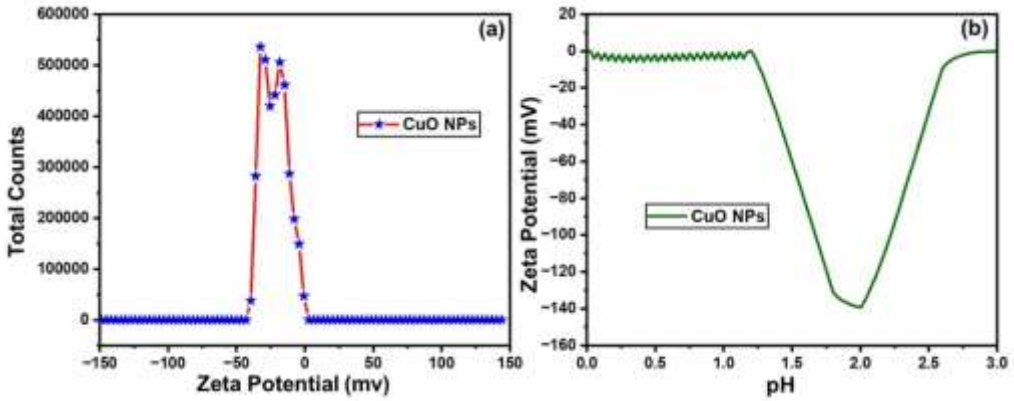

Fig.7. Zeta potential distribution of CuO NPs measured in aqueous medium (Milli-Q water, pH ~6.8) at 25 °C.

3.7. Cytotoxicity analysis

The *in vitro* cytocompatibility of *Padina tetrastromatica* extract, biosynthesized CuO NPs, and starch/PVA/CuO NPs electrospun nanoscaffolds was evaluated using the MTT assay on 3T3-L1 fibroblast cells. Cell viability was assessed over a concentration range of 6.25–100 µg/mL, and the results are expressed as percentage viability relative to untreated control cells. As shown in Fig. 8, all tested samples exhibited excellent cytocompatibility across the entire concentration range, with no evidence of dose-dependent cytotoxicity. At the highest tested concentration (100 µg/mL), cell viability values of 104.0 ± 5.2% for the algal extract, 106.0 ± 5.3% for CuO NPs, and 111.0 ± 5.6% for the starch/PVA/CuO nanoscaffolds were observed (mean ± SD, n = 3). Cell viability values exceeding 100% reflect enhanced mitochondrial metabolic activity rather than cytotoxic effects, indicating favorable short-term cellular responses. Overall, these results demonstrate that incorporation of green-synthesized CuO NPs into a starch/PVA electrospun matrix improves cytocompatibility compared to NPs alone.

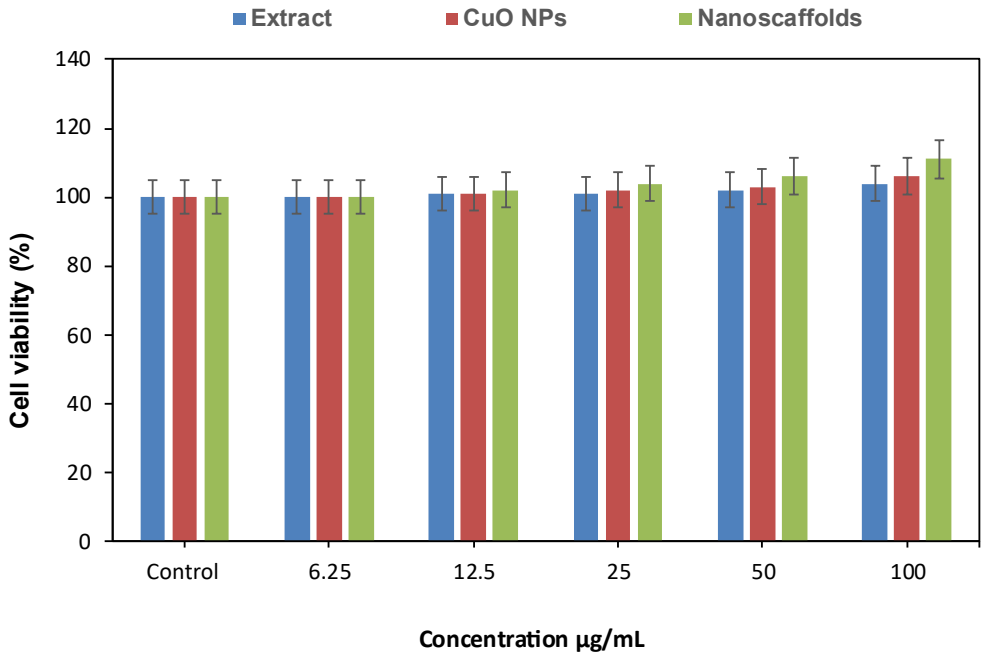

Fig.8. Cell viability of 3T3-L1 fibroblasts treated with algal extract, CuO NPs, and starch/PVA/CuO NPs nanoscaffolds for 24 h, expressed as mean ± SD (n = 3).

3.8. Free radical scavenging activity

3.8.1. DPPH Radical Scavenging Activity

The DPPH assay (Fig. 9) demonstrated the free radical scavenging potential of algal extract, CuO NPs, and starch/PVA/CuO NPs nanoscaffolds. At a concentration of 25 µg/mL, the algal extract exhibited 18.67% inhibition, while CuO NPs and nanoscaffolds showed 30.02% and 39.02% inhibition, respectively. As the concentration increased to 100 µg/mL, the scavenging activity significantly improved, with the extract reaching 69.82%, CuO NPs 76.22%, and nanoscaffolds 83.22%. The standard (Vitamin C) displayed the highest activity (89.05% at 100 µg/mL), confirming its superior antioxidant capacity. The results indicate that the nanoscaffolds

had the strongest DPPH scavenging effect among the tested samples, followed by CuO NPs and the algal extract. This suggests that the incorporation of CuO NPs into the polymeric matrix enhances antioxidant performance.

3.8.2. Nitric Oxide (NO) Scavenging Activity

The NO scavenging assay (Fig. 9) revealed that the algal extract, CuO NPs, and nanoscaffolds effectively neutralized nitric oxide radicals. At 25 µg/mL, the extract showed 11.68% inhibition, whereas CuO NPs and nanoscaffolds exhibited 18.02% and 24.02%, respectively. At higher concentrations (100 µg/mL), the extract achieved 69.50% inhibition, while CuO NPs and nanoscaffolds reached 75.22% and 79.22%, respectively. The standard (Vitamin C) displayed 84.41% inhibition at the same concentration. The nanoscaffolds again outperformed the individual components, indicating synergistic antioxidant effects due to the composite structure. The progressive increase in scavenging activity with concentration highlights a dose-dependent response.

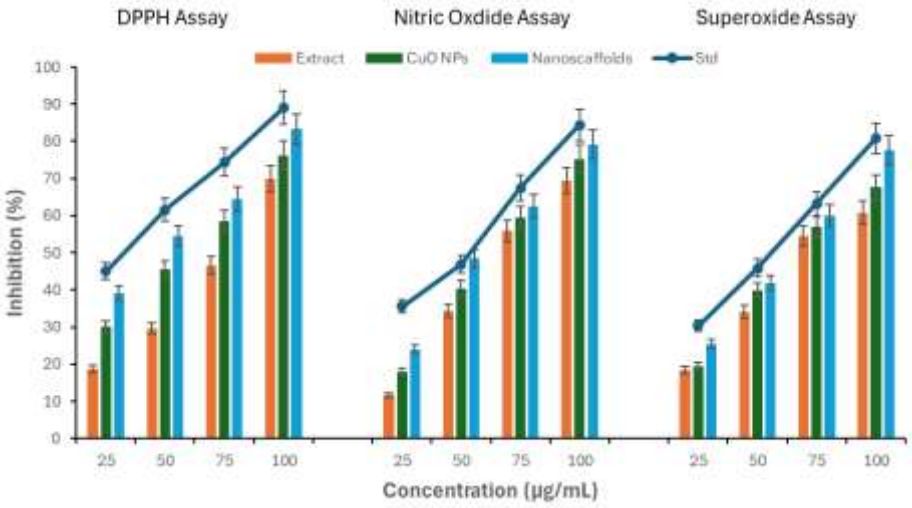

Fig.9. Dose-dependent antioxidant activity of algal extract, CuO NPs, and starch/PVA/CuO NPs nanoscaffolds evaluated by DPPH, nitric oxide, and superoxide radical scavenging assays. Results are expressed as mean ± SD (n = 3) at concentrations of 25–100 µg mL^{-1}, with ascorbic acid used as the standard (Std).

3.8.3. Superoxide Anion ($O_2^{\bullet-}$) Scavenging Activity

The superoxide radical scavenging assay (Fig. 9) demonstrated that all tested samples effectively reduced NBT to formazan, indicating $O_2^{\bullet-}$ neutralization. At 25 µg/mL, the algal extract exhibited 18.41% inhibition, while CuO NPs and nanoscaffolds showed 19.42% and 25.42%, respectively. At 100 µg/mL, the extract reached 60.80%, CuO NPs 67.62%, and nanoscaffolds 77.62%, compared to the standard (80.78%). The nanoscaffolds consistently displayed the highest activity, suggesting that the electrospun matrix enhances the dispersion and reactivity of CuO NPs, leading to improved radical scavenging.

Among all tested samples, the starch/PVA/CuO nanoscaffolds exhibited the lowest IC_{50} values (Table 1) across all antioxidant assays, indicating superior radical scavenging efficiency compared to CuO NPs alone and the algal extract. This enhancement can be attributed to the synergistic interaction between green-synthesized CuO NPs and the carbohydrate-based electrospun matrix, which may improve effective radical accessibility and stabilize redox-active sites.

Table 1: IC_{50} values of antioxidant activity of the algal extract, CuO NPs, and starch/PVA/CuO NPs nanoscaffolds

S. No	Assays	IC_{50} values (µg/mL)		
		S. ilicifolium Extract	CuO NPs	Starch/PVA/CuO Nanoscaffolds
1.	DPPH radical scavenging	78.68 ± 3.93	58.71 ± 2.94	42.82 ± 2.14
2.	Nitric oxide scavenging	68.20 ± 3.41	62.52 ± 3.13	52.78 ± 2.64
3.	Superoxide scavenging	69.52 ± 3.48	64.85 ± 3.24	61.27 ± 3.06

The antioxidant assays confirmed that the starch/PVA/CuO NPs nanoscaffolds possess superior scavenging activity compared to individual CuO NPs and algal extract. This enhancement is likely due to the synergistic effect of the polymeric support and nanoparticle integration. The dose-dependent behavior across all assays suggests that higher concentrations further improve antioxidant efficacy. These findings highlight the potential of nanoscaffolds in applications requiring advanced antioxidant materials.

4. DISCUSSION

The present study focused on the green synthesis of CuO NPs using *Padina tetrastromatica* extract and their incorporation into starch/PVA electrospun nanoscaffolds, followed by a comprehensive physicochemical and

biological evaluation. The UV–Visible spectroscopy confirmed the successful synthesis of CuO NPs, as evidenced by a prominent surface plasmon resonance (SPR) peak at 273 nm, a feature commonly associated with the formation of stable copper-based nanostructures [38-41]. The absence of a significant absorption peak in the algal extract spectrum suggests the unique optical behavior of the synthesized NPs, which results from nanoparticle formation and their electronic transitions. The SPR peak not only validates nanoparticle synthesis but also supports the involvement of bioactive molecules in reduction and stabilization, a hallmark of green synthesis methods [42-47].

FTIR spectroscopy provided further insight into the chemical nature and interactions of the CuO NPs and nanocomposites [48-53]. The distinct Cu–O stretching bands at ~602 cm^{-1} and ~433 cm^{-1} in the CuO spectrum confirmed metal-oxygen bond formation. Additionally, the presence of O–H and C=O functional groups indicates the potential role of biomolecules from the algal extract in nanoparticle stabilization. In the electrospun nanoscaffolds, characteristic peaks of both starch and PVA—such as O–H stretching, C–H bending, and C–O–C stretching—were clearly evident. These spectral features imply successful blending of the polymers. Notably, the lower wavelength peaks in the nanoscaffolds signify interactions between CuO NPs and polymer functional groups, validating the uniform distribution and integration of NPs within the biopolymeric matrix [54-59].

The structural properties were further confirmed by XRD analysis [60, 61]. The CuO NPs exhibited numerous sharp and intense peaks that correspond to the monoclinic tenorite phase of copper oxide, consistent with JCPDS 05-0661. The absence of extraneous peaks indicates high purity and crystallinity. In contrast, the starch/PVA nanoscaffolds showed a semi-crystalline structure with both broad and sharp peaks, representing an amorphous polymer matrix embedded with crystalline domains. These findings suggest that the integration of CuO NPs does not disrupt the structural integrity of the polymeric scaffold but rather contributes to a composite profile with potential functional benefits [62-69].

SEM analysis offered valuable morphological insights. The CuO NPs exhibited spherical to slightly irregular morphologies with good size uniformity, which is advantageous for biomedical applications. The starch/PVA electrospun scaffolds revealed a porous, interconnected fibrous network, a structural trait favorable for cell attachment, nutrient diffusion, and tissue regeneration. The smooth, bead-free nanofibers and uniform nanoparticle dispersion within the fibers highlight the efficiency of the electrospinning process. Furthermore, the absence of nanoparticle agglomeration implies good compatibility and interaction between the CuO and the polymeric matrix, contributing to the mechanical and functional stability of the scaffolds [70-74].

TGA provided data on thermal stability, an essential parameter for biomedical material development. The starch/PVA electrospun nanoscaffolds exhibited an onset of thermal degradation at approximately 298 °C and peak decomposition at 356.5 °C, consistent with the degradation temperatures of biopolymers. The substantial weight loss observed during this range is attributable to the breakdown of the starch and PVA backbones. The initial minor weight loss below 150 °C is likely due to the loss of moisture and volatile components. This degradation pattern supports the suitability of the scaffold for biomedical applications that do not require exposure to high temperatures, such as wound dressing or tissue engineering [75-77].

Zeta potential and DLS measurements were instrumental in evaluating colloidal stability and nanoparticle size distribution. The hydrodynamic diameter of CuO NPs averaged 108 nm, a value influenced by surface coatings and aggregation in solution. The moderately negative zeta potential (-22.13 mV) indicates fair colloidal stability, although values below -30 mV are typically required for high stability. Nevertheless, the measured zeta potential supports the formation of electrostatically stabilized suspensions, with the presence of surface-bound phytochemicals from the algal extract contributing to charge and dispersion properties. In the present system, the starch-PVA matrix should not be viewed as an inert carrier for CuO NPs, but rather as a hydrogen-bonded carbohydrate network that actively governs scaffold structure and functional response. Both starch and PVA possess abundant hydroxyl groups capable of forming intermolecular hydrogen bonds, leading to a semi-interpenetrating polymer network during electrospinning. This network plays a critical role in regulating solution viscosity, fiber formation, and nanoparticle immobilization within the fibrous matrix [78].

It is important to note that particle sizes derived from SEM, XRD, and DLS are not directly comparable due to fundamental differences in measurement principles. SEM provides physical particle dimensions in the dry state, XRD estimates crystallite size, and DLS measures hydrodynamic diameter, which includes solvation and surface-bound biomolecules. Therefore, the larger size observed in DLS measurements is expected and does not indicate inconsistency.

Biocompatibility was assessed using the MTT assay on 3T3-L1 preadipocyte cells. The *Padina tetrastromatica* extract, CuO NPs, and starch/PVA electrospun nanoscaffolds all exhibited excellent cytocompatibility, with viability consistently exceeding 100% across tested concentrations. Interestingly, the scaffolds not only supported cell viability but also appeared to enhance it at higher concentrations, suggesting a potential proliferative effect. This may be attributed to the favorable scaffold morphology and bioactive influence of the embedded NPs, indicating a promising platform for tissue engineering and regenerative medicine [79].

The antioxidant analysis of algal extract, CuO NPs, and starch/PVA/CuO NPs nanoscaffolds revealed significant differences in their radical scavenging capacities across DPPH, nitric oxide (NO), and superoxide anion ($O_2^{\bullet -}$) assays. In the DPPH assay, the nanoscaffolds exhibited the highest inhibition (83.22% at 100 µg/mL), surpassing both CuO NPs (76.22%) and the algal extract (69.82%), suggesting that the electrospun polymeric matrix enhances the antioxidant properties of CuO NPs, possibly through improved dispersion and stabilization of the

NPs. A similar trend was observed in the NO scavenging assay, where the nanoscaffolds (79.22%) outperformed CuO NPs (75.22%) and the extract (69.50%), reinforcing the role of the composite structure in facilitating radical neutralization. The superoxide assay further supported these findings, with the nanoscaffolds (77.62%) again demonstrating superior activity compared to CuO NPs (67.62%) and the extract (60.80%), likely due to the synergistic interaction between the starch/PVA matrix and the embedded NPs. Across all assays, the standard (Vitamin C or ascorbic acid) exhibited the highest activity, validating the experimental setup [80]. The dose-dependent increase in scavenging efficiency for all samples indicates that higher concentrations enhance antioxidant performance, with the nanoscaffolds consistently showing the most pronounced effects. These results highlight the potential of starch/PVA/CuO NPs nanoscaffolds as advanced antioxidant materials, where the composite design not only retains but amplifies the radical scavenging capabilities of its individual components, making it a promising candidate for biomedical and environmental applications requiring sustained oxidative stress mitigation [51, 52].

The results from this study validate the successful green synthesis of CuO NPs using *Padina tetrastromatica* extract and their effective incorporation into starch/PVA electrospun scaffolds. The multi-technique characterization confirms the desirable physical, chemical, thermal, and biological properties of the nanocomposite system. These findings position the developed nanoscaffold as a promising candidate for biomedical applications, particularly in areas requiring biocompatibility, antioxidant activity, and scaffold-based tissue regeneration.

The uniform, bead-free fiber morphology observed by SEM supports the presence of a stabilized polymer network during electrospinning. Such network-controlled fiber formation is critical for homogeneous CuO NPs dispersion, which in turn influences antioxidant accessibility and reduces localized nanoparticle-induced cytotoxic stress. Consequently, the observed antioxidant activity and favorable cytocompatibility should be interpreted as emergent properties of the starch-PVA hydrogen-bond network combined with green-synthesized CuO NPs, rather than as effects driven by CuO alone.

The improved antioxidant performance and cytocompatibility observed for the CuO NPs/starch/PVA electrospun mats should be interpreted in the context of the polymeric network rather than attributed solely to the presence of CuO NPs. The starch-PVA matrix provides a hydrophilic carbohydrate rich environment that promotes homogeneous nanoparticle distribution, limits NPs agglomeration, and reduces direct NPs cell contact. Such polymer-mediated modulation is known to influence surface accessibility and redox interactions, thereby contributing to enhanced functional performance. Importantly, the present results suggest a synergistic effect between the green-synthesized CuO NPs and the carbohydrate-based fibrous scaffold, rather than an isolated nanoparticle-driven response.

However, the present findings establish a sustainable route for integrating green-synthesized CuO NPs into a carbohydrate-based electrospun scaffold and demonstrate their antioxidant activity and cytocompatibility. While these results do not yet constitute application validation, they provide a foundational materials platform upon which application-specific benchmarks such as those required for wound dressing systems can be rigorously evaluated in future work.

5. LIMITATIONS AND FUTURE PROSPECTS

While this work demonstrates a preliminary materials level strategy for embedding green-synthesized CuO NPs within a starch/PVA electrospun matrix, several constraints limit application-level interpretation. Key performance indicators relevant to biomedical or wound related use such as antimicrobial efficacy, mechanical integrity, moisture vapor transmission (WVTR/MVTR), surface wettability, degradation behavior in physiological environments, copper-ion release kinetics, and in vivo biological response were not examined and therefore restrict definitive functional claims. The structural analyses relied primarily on qualitative evidence from FTIR and XRD, and quantitative elucidation of hydrogen bond interactions, crystallinity modulation, and polymer-nanoparticle coupling would require inclusion of neat polymer controls and complementary techniques such as DSC. Similarly, thermal analysis was confined to 550 °C without DTG profiling, preventing accurate determination of inorganic residue and CuO loading. In addition, the absence of polymer-only, polymer CuO binary, and extract only controls limits the ability to decouple the individual contributions of each component to the observed antioxidant activity and cytocompatibility. Addressing these gaps through systematic mechanical testing, WVTR/MVTR measurements, antimicrobial assays against relevant pathogens, copper-release profiling, degradation studies, expanded thermal analysis, and inclusion of appropriate material controls will be essential to establish robust structure-property-bioactivity relationships and to advance this system beyond a proof-of-concept toward application-ready validation.

6. CONCLUSION

This study establishes a carbohydrate-centric materials proof-of-concept for integrating green-synthesized CuO NPs within a starch/PVA electrospun nanofibrous matrix. The hydrogen-bonded starch/PVA network facilitated uniform fiber formation and effective immobilization of CuO NPs, which together translated into favorable biological responses. The resulting nanoscaffolds demonstrated moderate cytocompatibility, with 111.0 ± 5.6% cell viability at 100 µg/mL (n = 3), and enhanced antioxidant performance, as reflected by low IC_{50} values of 42.82 ± 2.14 µg/mL (DPPH), 52.78 ± 2.64 µg/mL (NO), and 61.27 ± 3.06 µg/mL (superoxide). These outcomes

indicate that the carbohydrate network plays an active role in moderating CuO redox accessibility and mitigating NPs induced cytotoxic stress, rather than acting as a passive carrier. Importantly, application-defining metrics including mechanical strength, WVTR/MVTR, antimicrobial efficacy, degradation behavior, and Cu^{2+} release kinetics were not assessed and therefore preclude definitive biomedical or wound-care claims at this stage. Next steps to advance this system toward application validation include: quantifying tensile and WVTR properties; testing antimicrobial activity against pathogenic microbes and measuring Cu^{2+} release profiles to mechanistically link ion availability with observed antioxidant and cell responses.

Funding: This study was funded by Lucian Blaga University of Sibiu & Hasso Plattner Foundation research grants LBUS-IRG-2022-08.

Data Availability Statement: The full dataset of physiochemical characterization associated with this work is published in Mendeley Data [Dataset] *Padina tetrastromatica*-driven synthesis meets biopolymers: comprehensive profiling of starch nanoscaffolds infused with eco-friendly copper oxide nanoparticles (DOI: 10.17632/ddbgcpm32x.1). Disclosure: The material characterization data and figures (e.g., UV, SEM, FTIR, XRD, TGA, Zeta Potential and particle sizer) presented here were generated from a common dataset and are being reused across multiple related studies on nanomaterials. All biological analyses and conclusions are original to each manuscript.

Conflicts of Interest: The authors declare no conflicts of interest.

REFERENCES

[1] Natarajan PM, Swamikannu B, Sivaraman NM, Stylin AGSQ. Prevention of Oral Cancer: A Comprehensive Guide. Journal of Pharmacy and Bioallied Sciences. 2024; 16(5): S4239-S4241.
[2] Umapathy V, Dhanavel A, Kesavan R, Natarajan PM, Bhuminathan S, Vijayalakshmi P. Anticancer Potential of the Principal Constituent of Piper nigrum, Piperine: A Comprehensive Review. Cureus. 2024; 16(2): e54425.
[3] Umapathy VR, Swamikannu B, Natarajan PM, Devi R, Nandini MS, Vimalarani, Vijayalakshmi P. In Silico Molecular Docking of Ocimum sanctum Phytochemicals: Targeting Key Biomarkers in Oral Cancer. Journal of Pharmacy and Bioallied Sciences. 2024; 16(5): S4792-S4799.
[4] Natarajan PM, Bhuminathan S, Rajan R, Bindu K, Loganathan K, Veerakumar R. The Crucial Role of Smoking Cessation in Preventing Oral Cancer. Journal of Pharmacy and Bioallied Sciences. 2024; 16(5): S4245-S4247.
[5] Swamikannu B, Umapathy VR, Natarajan PM, Nandini MS, Stylin AGSQ, Vimalarani V, Rajinikanth S. Unlocking the Therapeutic Benefits of Artemisia Annua: A Comprehensive Overview of its Medicinal Properties. Journal of Pharmacy and Bioallied Sciences. 2024; 16(5): S4248-S4253.
[6] Natarajan PM. Computational Studies on Recent Congeners of Fluoroquinolones and Nitroimidazoles for Their Use in Periodontal Therapy. Journal of Pharmacy and Bioallied Sciences. 2024; 16(5): S4731-S4740.
[7] Yadalam PK, Arumuganainar D, Natarajan PM, Ardila CM. Artificial intelligence-powered prediction of AIM-2 inflammasome sequences using transformers and graph attention networks in periodontal inflammation. Scientific Reports. 2025; 15: 8733.
[8] Yadalam PK, Chatterjee S, Natarajan PM, Ardila CM. Comparison of light gradient boosting and logistic reg ression for interactomic hub genes in Porphyromonas gingivalis and Fusobacterium nucleatum-induced periodo ntitis with Alzheimer's disease. Frontiers in Oral Health. 2025; 6:1463458.
[9] Natarajan PM, Bhuminathan S, Leela B, Bindu K, Loganathan K, Ramachandran V. Smoking and its Role in Oral Cancer. Journal of Pharmacy and Bioallied Sciences 16(5): S4242-S4244.
[10] Yadalam PK, Natarajan PM, Ardila CM. Variational graph autoencoder for reconstructed transcriptomic data associated with NLRP3 mediated pyroptosis in periodontitis. Scientific Reports. 2025; 15: 1962.
[11] Pei JJ, Perumal NC, Meng P, Long Q, Palanisamy CP. AI-assisted FTIR spectroscopic profiling of exosomes: Emerging frontiers in early detection of Alzheimer's disease. Ageing Research Reviews. 2026; 103311.
[12] Raja FSD, Abraham L, Rangasamy K, Saikia K, Rathankumar AK, Mironescu M, Mironescu I, Palanisamy CP, Kanniappan GV. Next-Generation Microbiome Therapeutics: Psychobiotics and Fecal Microbiota Transplants (FMT) for Mental Health Treatment. Frontiers in Cellular and Infection Microbiology. 2026; 16: 1719357.
[13] Subramani K, Srinivasan S, Shanmugam P, Palanisamy CP, Sonsudin F, Poompradub S. Sustainable phytochemical mediated-ZnO nanoparticles derived from Crescentia cujete for toxicological evaluation and multifunctional environmental applications. Environmental Nanotechnology, Monitoring & Management. 2026; 26: 101180.
[14] Kunamalla RP, Panagal M, Palanisamy CP. Green-engineered multiscale starch/PVA nanofibrous scaffolds embedded with CuO nanoparticles from Sargassum ilicifolium for potent antimicrobial performance. Genetics and Molecular Research. 2026; 25(13s): 1-9.
[15] Dharmaprakash S, Gunasekaran VP, Sivaramakrishnan R, Kanniappan GV, Jayaraman S, Mironescu M, Rajabathar JR, Mironescu ID, Palanisamy CP. Marine macroalgae-mediated ultrasonic-assisted green synthesis

of CuO nanoparticles embedded in starch/PVA electrospun nanoscaffolds for in vitro α-amylase and α-glucosidase inhibitory activity. Scientific Reports. 2026; 16: 26243.
[16] Surendran N, Chandrasekaran G, Raju MV, Chandrasekaran MK, Ahalliya RM, Palanisamy CP, Kanniappan GV, Arcot R, Alharbi NS, Thiruvengadam M. Anti-inflammatory potential of ethanolic extract of Maranta arundinacea L.: Insights from COX-2 modulation and oxidative stress analysis. South African Journal of Botany. 2026; 195: 142-151.
[17] Pei J, Senthilkumar MV, Hessini K, Subramaniyam S, Sivaramakrishnan R, Kanniappan GV, Jayaraman S, Palanisamy CP. Green fabrication of starch/PVA/CuO nanoscaffolds using marine macroalgae extract for enhanced anti-inflammatory activity. Sustainable Chemistry and Pharmacy. 2026; 51: 102397.
[18] Balasubramanian V, Loganathan L, Muthuswamy K, Viswanathan TM, Raju MV, Chandrasekaran MK, Ahalliya RM, Poorasamy J, Palanisamy CP, Dominic S, Kanniappan GV. Anticancer therapeutic efficacy of PEGylated β-galactosidase from Aspergillus terreus in DMBA-induced breast cancer: Toxicological, molecular and histopathological evaluation in Wistar rats. International Journal of Biological Macromolecules. 2026; 360: 151856.
[19] Jayaraman S, Eswaran A, Rajagopal P, Palanisamy CP, Veerakumar P, Veeraraghavan VP, Sirasanagandla SR. Neuroendocrine-associated epigenetic factors in cellular senescence: mechanisms and therapeutic implications. Biogerontology. 2026; 27(2): 64.
[20] Ponnusamy B, Rajagopal P, Palanisamy CP, Veeraraghavan VP, Jayaraman S. Mechanistic Exploration of the anticancer activity of Justicia adhatoda Plant Leaf Ethanolic Extract against Colon Cancer Cells: An in silico and in vitro Approach. Asian Pacific Journal of Cancer Prevention. 2026; 27(3): 1069-1080.
[21] Pei J, Saran VS, Sivaramakrishnan R, Kanniappan GV, Pandurangan V, Jayaraman S, Dhayalan VK, Mironescu M, Mironescu ID, Palanisamy CP. Ultrasonic-assisted, Sargassum ilicifolium (brown marine macroalgae)-mediated biogenic synthesis of CuO nanoparticles incorporated in starch/PVA electrospun nanoscaffolds: In vitro safety and antioxidant efficacy assessment. Bioorganic Chemistry. 2026; 173: 109679.
[22] Raj MAPA, Subramaniyam S, Kanniappan GV, Jayaraman S, Palanisamy CP. Sustainable fabrication of starch/PVA/CuO electrospun nanoscaffolds from Turbinaria ornata (marine macroalgae) extract: Physicochemical characterization and antidiabetic evaluation. Kuwait Journal of Science. 2026; 53(2): 100545.
[23] Pei J, Ganesh NS, Subramaniyam S, Sivaramakrishnan R, Kanniappan GV, Jayaraman S, Palanisamy CP. Sustainable fabrication of starch/PVA/CuO electrospun nanoscaffolds from Padina tetrastromatica (Brown macroalgae) extract: Physicochemical characterization and antidiabetic assessment. Sustainable Chemistry One World. 2026; 9: 100195.
[24] Sakthiraj A, Sivaramakrishnan R, Subramaniyam S, Kanniappan GV, Pandurangan V, Jayaraman S, Dhayalan VK, Mironescu M, Mironescu ID, Palanisamy CP. Starch/PVA electrospun nanoscaffolds loaded with ultrasonic-assisted green-synthesis of CuO nanoparticles from marine macroalgae (Gracilaria corticata) extract: Cytotoxicity and antioxidant analysis. Chemical Physics Impact. 2026; 12: 101018.
[25] Raju M, Chandrasekaran MK, Loganathan L, Ahalliya RM, Mironescu M, Mironescu ID, Palanisamy CP, Kanniappan GV. Lipid remodeling and ferroptosis in phosphatidylcholine-mediated tumor–stroma crosstalk. Frontiers in Molecular Biosciences. 2026; 13: 1742305.
[26] Kunamalla R, Panagal M, Palanisamy CP. Biogenic synthesis and fabrication of starch/PVA/CuO electrospun nanoscaffolds from Sargassum ilicifolium (brown marine macroalgae) extract for anticancer activity on HT-29 and MCF-7 cancer cells. Biocatalysis and Agricultural Biotechnology. 2026; 72: 103923.
[27] Pei J, Govindaraj H, Sivaramakrishnan R, Kanniappan GV, Pandurangan V, Dhayalan VK, Mironescu M, Mironescu ID, Jayaraman S, Palanisamy PC. Sustainable fabrication of biopolymer-based (starch/PVA) nanoscaffolds loaded with green-synthesized CuO nanoparticles from Sargassum wightii (marine macroalgae): Cytocompatibility and antioxidant activity. Biomaterials Advances. 2026; 182: 214660.
[28] Pei J, Perumal NC, Meng P, Long Q, Palanisamy CP. Extracellular vesicle-based biosensors for Alzheimer's disease: A new frontier in precision diagnostics. Ageing Research Reviews. 2026; 113: 102904.
[29] Shree P, Sivaramakrishnan R, Kanniappan GV, Pandurangan V, Jayaraman S, Dhayalan VK, Mironescu M, Mironescu ID, Palanisamy CP. Antioxidant and biocompatible CuO-starch/PVA nanoscaffolds via ultrasonic green synthesis using Turbinaria conoides (brown marine macroalgae). Medicine in Drug Discovery. 2025; 28: 100238.
[30] Gong J, Lin J, Guan T, Pei J, Palanisamy CP, El-AtyFrom AMA. selenium tolerance to nanoplastic antagonism: Comprehensive characterization of L. casei SNUT1 and its extracellular vesicle–nanoselenium complex. Food Bioscience. 2025; 74: 107749.
[31] Poochi SP, Sundarraj R, Raju MV, Chandrasekaran MK, Ahalliya RM, Palanisamy CP, Kanniappan GV, Kondapavuluri BK, Thiruvengadam M. Harnessing Nature: Computational and Experimental Insights Into *Ipomoea obscura* Metabolites for Bladder Cancer Therapy. Chemistry and Biodiversity. 2025; 0: e00909.
[32] Dugganaboyana GK, Kannankumar MKG, Shivaramakrishna S, Raju MV, Chandrasekaran MK, Ahalliya RM, Panneerselvam N, Palanisamy CP, Kanniappan GV. Phytochemical insights, antioxidant activity and therapeutic potential of Cassia senna against prostate cancer in Wistar albino rats. Discover Applied Sciences. 2025; 7:1206.
[33] Natarajan SR, Krishnamoorthy R, Alshuniaber MA, Gatasheh MK, Rajagopal P, Veeraraghavan VP, Palanisamy CP, Jayaraman S. KDM1A Facilitates Oncogenic Potential in Colorectal Cancer Progression

Through the Activation of AXIN/GSK3β/β-Catenin Signaling Pathways: Evidence From Integrated Transcriptomics and In Vitro Studies. The Journal of Gene Medicine. 2025; 27(11): e70053.
[34] Guan T, Gong J, Lin J, Palanisamy CP, Jinjin Pei J, El-Aty AMA. Machine learning-driven multimodal optimization of selenium biotransformation and flavor profiling in fermented apple–Yacon functional beverages. Innovative Food Science & Emerging Technologies. 2025; 105: 104198.
[35] Natarajan SR, Krishnamoorthy R, Alshuniaber MA, Alsulami TS, Gatasheh MK, Rajagopal P, Palanisamy CP, Govindan R, Veeraraghavan VP, Jayaraman S. ABCE1 facilitates tumour progression via aerobic glycolysis and inhibits cell death in human colorectal cancer cells through the p53 signalling pathway. Scientific Reports. 2025; 15: 24674.
[36] Huang Y, Guo H, Liu Y, Jin W, Palanisamy CP, Pei J, Oz F, El-Aty AMA. Effects of Natural Polysaccharides on the Gut Microbiota Related to Human Metabolic Health. Molecular Nutrition & Food Research. 2025; 69:e202400792.
[37] Poornima K, Meenakshi K.C, Manikandan V.R, Shankari G, Prabhu D, Rathi M.A, Palanisamy CP, Balaji R, Gopalakrishnan V.K. Exploring the anticancer potential of Jerantinine A from *Tabernaemontana coronaria* against prostate, breast, and ovarian cancers: A computational approach. *Journal of Complementary and Integrative Medicine*, 2025 22(2): 363–372.
[38] Palanisamy CP, Poompradub S, Sansanaphongpricha K, Jayaraman S, Subramani K. Faridah Sonsudin gGreen synthesis of Nigella sativa-mediated silver nanoparticles for enhanced antibacterial activity and wound healing: Mechanistic insights and biomedical applications. Environmental Nanotechnology, Monitoring & Management. 2025; 24: 101085.
[39] Surendran N, Raju MV, Chandrasekaran MK, Ahalliya RM, Palanisamy CP, Chandrasekaran G, Kanniappan GV. Physicochemical characterization of starch from Maranta arundinacea L.(arrowroot) rhizomes and its inhibition of COX-2: In vivo validation. Bioactive Carbohydrates and Dietary Fibre. 2025; 33: 100465.
[40] Natarajan PM, Umapathy VR, Murali A, Swamikannu B. (2022). Computational Simulations of Identified marine-derived Natural Bioactive Compounds As Potential Inhibitors of Oral Cancer. Future Science OA. 2022; 8(3).
[41] Natarajan PM, Umapathy VR. Role of transcriptomics in the study of oral cancer. Frontiers in Oral Health. 2025; 6:1524364.
[42] Vidhyarekha U, Natarajan PM, Bhuminathan S, Sabarinathan J, Suba R, Vijayalakshmi P. Role of artificial intelligence in Oral Cancer. Advances in Public Health. 2024. 2024: 3664408.
[43] Ganesan A, Kumar NG, Natarajan PM, Gauthaman J. Automated classification of elongated styloid processes using deep learning models-an artificial intelligence diagnostics. Frontiers in Oral Health. 2025; 5: 1424840.
[44] Umapathy VR, Natarajan PM, Swamikannu B. Regenerative Strategies in Dentistry: Harnessing Stem Cells, Biomaterials and Bioactive Materials for Tissue Repair. Biomolecules. 2025; 15: 546.
[45] Natarajan PM. Dental Bioinformnatics-Current Scope and Future perspectives. Research Journal of Pharmacy and Technology. 2022;15(5):2351-6.
[46] Ganesan A, Kumar NG, Natarajan PM. Solanum trilobatum leaf extract-derived silver nanoparticles downregulate the PI3K/AKT/mTOR signaling pathway and attenuate oral squamous cell carcinoma cell proliferation. Journal of Herbmed Pharmacology. 2024; 13(2): 300-307.
[47] Perumal MKK, Renuka RR, Subbiah SK, Natarajan PM. Artificial intelligence-driven clinical decision support systems for early detection and precision therapy in oral cancer: a mini review. Frontiers in Oral Health. 2025; 6: 1592428.
[48] Ramesh E, Ganesan A, Lakshmi KC, Natarajan PM. Artificial intelligence-based diagnosis of oral leukoplakia using deep convolutional neural networks Xception and MobileNet-v2. Frontiers in Oral Health. 2025; 6: 1414524.
[49] Ganesan A, Kumar NG, Natarajan PM. Anticancer activity of silver nanoparticles synthesized from aqueous leaf extract of Solanum trilobatum (Purple fruit pea eggplant) on human oral cancer cells. Journal of Herbmed Pharmacololgy. 2024; 13(2): 260-268.
[50] Kannappan P, Chandrasekaran MK, Raju MV, Gopalakrishnan S, Dhamodharan P, Ahalliya RM, Palanisamy CP, Raju B, Kanniappan GV. Exploring the anticancer potential of Jerantinine A from Tabernaemontana coronaria against prostate, breast, and ovarian cancers: a computational approach. Journal of Complementary and Integrative Medicine. 2025; 22(02): 363-372.
[51] Pei J, Kumarasamy RV, Jayaraman S, Kanniappan GV, Long Q, Palanisamy CP. Quercetin-functionalized nanomaterials: Innovative therapeutic avenues for Alzheimer's disease management. Ageing Research Reviews. 2025; 104: 102665.
[52] Jayaraman S, Prasad M, Natarajan SR, Krishnamoorthy R, Alshuniaber MA, Gatasheh MK, Veeraraghavan VP, Rajagopal P, Palanisamy CP. Molecular mechanisms underlying the effects of beta-sitosterol on TGF-β1/Nrf2/SIRT1/p53-mediated signaling in the kidney of a high-fat diet and sucrose-induced type-2 diabetic rat. Chemico-Biological Interactions. 2025; 411: 111443.
[53] Huang Y, Guo H, Liu Y, Jin W, Palanisamy CP, Pei J, Oz F, El-Aty AMA. Effects of Natural Polysaccharides on the Gut Microbiota Related to Human Metabolic Health. Molecular Nutrition & Food Research. 2025; e202400792.

[54] Prabhakaran P, Palanisamy CP, Shanmugam A, Damodharan P, Swaminathan H, Devaraj D, Ahalliya RM, Kanniappan GV. Isolation, structural characterization, and molecular docking studies on the bioactive compound from n-Hexane extract of Emilia sonchifolia (L.) DC against the pancreatic cancer target Aurora 2 Kinase. Journal of Complementary and Integrative Medicine. 2024; 22(1): 0290.
[55] Jiang H, Kumarasamy RV, Pei J, Raju K, Kanniappan GV, Palanisamy CP. Integrating engineered nanomaterials with extracellular vesicles: Advancing targeted drug delivery and biomedical applications. Frontiers in Nanotechnology. 2024; 6: 1513683.
[56] Guo H, Liu Y, Wan T, Song D, Palanisamy CP, Geng J, Pei J, Özmen S, El-Aty AMA. Toward personalized cancer management: Role of precision nutrition–diet interventions. Journal of Functional Foods. 2024; 123: 106584.
[57] Natarajan SR, Krishnamoorthy R, Alshuniaber MA, Al-Anazi KM, Farah MA, Rajagopal P, Palanisamy CP, Veeraraghavan VP, Jayaraman S. Identification of FOXM1 as a novel protein biomarker and therapeutic target for colorectal cancer progression: Evidence from immune infiltration and bioinformatic analyses. International Journal of Biological Macromolecules. 282 (Part 4): 137201.
[58] Rajendran MS, Jayaraman S, Khan JM, Jasmine S, Prabhakaran RK, Raju MV, Chandrasekaran MK, Ahalliya RM, Kannappan P, Palanisamy CP, Kanniappan GV. Investigating the colon toxicity and carcinogenic role of monosodium glutamate compared with Dimethylhydrazine in male Wistar rats: Exploring the link to childhood colon cancer risk. Journal of King Saud University - Science. 2024; 36(11): 103507.
[59] Kumarasamy RV, Natarajan P, Umapathy VR, Roy JR, Rab SO, Saeed M, Panagal M, Mironescu M, Srinivasan GP, Palanisamy CP. Clinical Applications and Therapeutic Potentials of Advanced Nanoparticles: A Comprehensive Review on Completed Human Clinical Trials. Frontiers in Nanotechnology. 2024; 6:1479993.
[60] Jin W, Pei JJ, Roy JR, Jayaraman S, Ahalliya RM, Kanniappan GV, Mironescu M, Palanisamy CP. Comprehensive review on single-cell RNA sequencing: A new frontier in Alzheimer's disease research. Ageing Research Reviews. 2024; 274: 102454.
[61] Pei J, Palanisamy CP, Jayaraman S, Natarajan PM, Umapathy VR, Roy JR, Panagal M, Jayaraman S. Curcumin-loaded polymeric nanomaterials as a novel therapeutic strategy for Alzheimer's disease: A comprehensive review. Ageing Research Reviews. 2024; 99: 102393.
[62] Pei J, Palanisamy CP, Jayaraman S, Natarajan PM, Umapathy VR, Roy JR, Thalamati D, Ahalliya RM, Kanniappan GV, Mironescu M. A comprehensive review on starch-based Sustainable Edible Films Loaded with Bioactive Components for Food Packaging. International Journal of Biological macromolecules. 2024; 274 (Part-1): 133332.
[63] Palanisamy CP, poompradub S, Sansanaphongpricha K, Subramani K, Sonsudin F. Increased expression levels of PDGF and VEGF magnify the wound healing potential facilitated by biogenic synthesis of silver nanoparticles. Nano-Structures & Nano-Objects. 2024; 39: 101236.
[64] Pei J, Palanisamy CP, Jayaraman S, Natarajan PM, Umapathy VR, Roy JR, Thalamati D, Ahalliya RM, Kanniappan GV, Mironescu M. Proteomics Profiling of Extracellular Vesicle for Identification of Potential Biomarkers in Alzheimer's Disease: A Comprehensive Review. Ageing Research Reviews. 2024; 99: 102359.
[65] Xi J, Wang T, Xian P, Liu X, Du M, Yang H, Palanisamy CP, Lin W, Long Q. Proteomic insights uncover enhanced neurotherapeutic potential in conditioned mesenchymal stem cell-derived extracellular vesicles. Extracellular Vesicle. 2024; 3: 100037.
[66] Pei J, Natarajan PM, Umapathy VR, Swamikannu B, Sivaraman NM, Krishnasamy L, Palanisamy CP. Advancements in the synthesis and functionalization of zinc oxide-based nanomaterials for enhanced oral cancer therapy. Molecules. 2024; 29(11): 2706.
[67] Gatasheh MK, Natarajan SR, Krishnamoorthy R, Alsulami TS, Rajagopal P, Palanisamy CP, Veeraraghavan VP, Jayaraman S. Molecular analysis to identify novel potential biomarkers as drug targets in colorectal cancer therapy: an integrated bioinformatics analysis. Molecular and Cellular Oncology. 2024; 11(1): 2326699.
[68] Pei J, Yan Y, Jayaraman S, Rajagopal P, Natarajan PM, Umapathy VR, Gopathy S, Roy JR, Sadagopan CS, Thalamati D, Palanisamy CP, Mironescu M. A review on advancements in the application of starch-based nanomaterials in biomedicine: Precision drug delivery and cancer therapy. International Journal of Biological Macromolecules. 2024; 130746.
[69] Pei JJ, Yan Y, Palanisamy CP, Jayaraman S, Natarajan PM, Umapathy VR, Gopathy S, Roy JR, Sadagopan JC, Thalamati D, Mironescu M. Materials-based drug delivery approaches: Recent advances and future perspectives. Green Processing and Synthesis. 2024; 13: 20230094.
[70] Pei JJ, Deng W, Liu Y, Guo Y, Chen J, Abdu H, Khan MR, Palanisamy CP, El-Aty AM. A Comprehensive Review of Cornus officinalis: Health Benefits, Phytochemistry, and Pharmacological Effects for Functional Drug and Food Development. Frontiers in Nutrition. 2023; 10: 1309963.
[71] Alugoju P, Palanisamy CP, Anthikapalli NVA, Jayaraman S, Prasanskulab A, Chuchawankul S, Dyavaiah M, Tencomnao T. Exploring the anti-aging potential of natural products and plant extracts in budding yeast Saccharomyces cerevisiae: A review. F1000Research. 2023; 12: 1265.
[72] Lavanya M, Krishnamoorthy R, Alshuniaber MA, Manoharadas S, Palanisamy CP, Veeraraghavan VP, Jayaraman S, Rajagopal P, Padmini R. Formulation, characterization and evaluation of gelatin-syringic acid/zinc oxide nanocomposite for its effective anticancer, antioxidant and anti-inflammatory activities. Journal of King Saud University-Science. 2023; 35: 102909.

[73] Palanisamy CP, Poompradub S, Sansanaphongpricha K, Jayaraman S, Subramani K, Sonsudin F. Biosynthesis of silver nanoparticles (AgNPs) using ethanolic extract of Nigella sativa (L.) seeds promotes wound healing via PDGF and VEGF signalling pathways activation. Biocatalysis and Agricultural Biotechnology. 2023; 54: 102970.
[74] Prasad M, Jayaraman S, Natarajan SR, Veeraraghavan VP, Krishnamoorthy R, Gatasheh MK, Palanisamy CP, Elrobh M. Piperine modulates IR/Akt/GLUT4 pathways to mitigate insulin resistance: Evidence from animal and computational studies. International Journal of Biological Macromolecules. 2023; 253: 127242.
[75] Palanisamy CP, Pei JJ, Phaniendra A, Venkata AAN, Jayaraman S, Veeraragahavan VP, Sridevi G, Roy JR, Janaki CS, Thalamati D, Mironescu M, Luo Q, Chai Y, Long Q. New Strategy of Neurodegenerative Disease Treatment with Extracellular Vesicles (EVs) Derived from Mesenchymal Stem Cells (MSCs). *Theranostics*. 2023; 13(12):4138-4165. doi:10.7150/thno.83066.
[76] Palanisamy CP, Phaniendra A, Jayaraman S, Poompradub S. *Nigella sativa* L. seed extracts promotes wound healing progress by activating VEGF and PDGF signalling pathways: *An in vitro* and *in silico* study. *F1000 Research*. 2023; 12: 436.
[77] Pei JJ, Palanisamy CP, Phaniendra A, Venkata AAN, Natarajan PM, Umapathy VR, Swamikannu B, Jayaraman S, Rajagopal P, Poompradub S. A comprehensive review on bio-based materials for chronic diabetic wounds. *Molecules*. 2022; 28(2), 604.
[78] Palanisamy CP, Cui B, Zhang H, Gunasekaran VP, Ariyo A, Jayaraman S, Veeraraghavan V, Rajagopal P. A critical review on starch-based electrospun nanofibrous scaffolds for wound healing application. International Journal of Biological Macromolecules. 2022; 222 (Part: B): 1852-1860.
[79] Monisha P, Ponnulakshmi R, Nalini D, Vishnu P V, Palanisamy CP, Cui B, Shankargouda P, Selvaraj J. A comprehensive review on high fat diet-induced diabetes mellitus: An epigenetic view. The Journal of Nutritional Biochemistry. 2022; 2022: 109037.
[80] Monisha P, Selvaraj J, Mohamed AE, Mohamed E, Mosaab AEA, Vishnu PV, Srinivasan V, Vidhya RU, Shazia FJH, Kalaiselvi K, Durairaj S, Palanisamy CP, Surapaneni K M, Ponnulakshmi R. A Comprehensive review on therapeutic perspectives of phytosterols in insulin resistance: A mechanistic approach. Molecules. 2022; 27(5): 1595.